ISSN: 2454-1907
DOI: https://doi.org/10.29121/ijetmr.v5.i8.2018.277

IJETMR
International Journal of Engineering Technologies and Management Research
A Knowledge Repository

NUMERICAL ANALISIS OF THE STRAINS AND STRESS STATES REINFORCED CLAY BRICK MASONRY WALLS HORIZONTALLY SHEARED

Radosław Jasiński [*1]
[*1] Building Structures Department, Silesian University of Technology, Poland

Abstract:
This paper presents the results: stress and strain of bed joints mortar, masonry units, reinforcement bars and mechanism of cracking of numerical simulations using ANSYS of reinforced brick wall in the horizontal shear. Willam-Warnke (WW-5) failure criterion for mortar and bricks and Huber-Mises-Hencky (HMH) plasticity surface for bed joints steel reinforcement (steel smooth bars and truss type reinforcement) has been used. Coulomb-Mohr (CM) criterion in the contact surfaces of mortar and bricks have been used in the interface elements. Numerical calculations showed satisfactory convergence of research in the patterns of cracking; and the load-strain relationship was similar to the results of research with regard only to the cracking time. Destructive force numerical models Hu,cal correspond to the forces observed at the first cracks in the walls Hu,mv. Reduction of transverse and longitudinal deformation of mortar bed joints have been reported in the immediate vicinity of the bars, and the reduction of the main stress of the bricks is reported in the case of the use reinforcement.

Keywords: Reinforced Masonry Structures; Horizontal Shear Wall; FEM Analysis; Discrete Micro Model; Interface Element; Willam-Warnke Model.

Cite This Article: Radosław Jasiński. (2018). "NUMERICAL ANALISIS OF THE STRAINS AND STRESS STATES REINFORCED CLAY BRICK MASONRY WALLS HORIZONTALLY SHEARED." *International Journal of Engineering Technologies and Management Research*, 5(8), 20-37. DOI: https://doi.org/10.29121/ijetmr.v5.i8.2018.277.

1. Introduction

The FEM analysis allows tracing of the work of construction of the linear range, by cracking until its destruction. Nonlinear material models based on experimental observations, different constitutive relationships and failure criteria are mainly used. Several different modeling methods in terms of the complexity of real masonry construction can be identified. Micromodel is the most complex method of modeling the masonry structure. The test samples are treated as a heterogeneous material with reinforcement taking into account issues of contact between the mortar and the masonry units. Different non-linear behavior of brick, mortar and the reinforcement used in this case ([1,2,3,4,5,6,7,8,19]. For macromodel and mezomodel characterized by lower complexity, the wall has the same mechanical properties of the periodic structure [18], these models may be used in the practical calculations of large masonry structures, not just parts of the wall, but also whole buildings [1,9,10,2,3,5,6,11,12,13, 14]. Reinforcement of the macromodel walls are modeled as a linear elements, representing the reinforcement bars

ISSN: 2454-1907
DOI: 10.5281/zenodo.1412216

[8,19,4] or with reinforced bed joints changing the mechanical properties [18, 20]. Theoretical analysis of reinforced walls suggest that the local deformations of the mortar reduced due to the presence of reinforcement will increase the intensity of cracking joints and increase the value of the cracking stress. The most positive impact of reinforcement is visible in the walls under compression. A study of 51 clay brick walls [22] also confirmed the significant influence of reinforcement.

To recognize influence of reinforcement it was necessary to build a FEM numerical model of the fragment wall, allowing for a detailed analysis of the interaction of mortar and masonry reinforcement until the cracking state. The main aim of this study was to conduct numerical analysis of the results of research [22] in terms of:

- patterns of cracking,
- influence of reinforcement on the mortar strains,
- values of cracking and destructive forces,
- principal stress (σ_1) in the bricks.

2. Numerical Model of the Wall

2.1. Modeling Strategy

Analysis of the stress and strain states were carried out on a separate fragment wall of the central area of the research model. Due to the limited technical possibilities, the calculation process is divided into 3 stages.

- Stage I. Numerical model of the wall sheared horizontally (orthotropic shell model) the real size was built. Models were initially compressed to obtain stress σ_c = 0 and 1.5 N/mm^2 depending on the series of elements and sheared the horizontal force *H*. Displacement of *n* nodes ($^{0, x_n^I, z_n^I}$) lying around the edges of the middle, mentally separate parts of 600 × 600 mm, located in the central area of the wall [22] - Figure 1 have been identified on the basis calculations.
- Stage II. Displacements of *n* nodes ($^{0, x_n^I, z_n^I}$) lying on the edge of the part 600 × 600 mm obtained from stage I was loaded linear-elastic solid numerical micromodels of wall (unreinforced, reinforced with bars and truss type reinforcement) overall dimensions 600 × 600 × 250 (125) mm. Eight nodes finite elements were used in this stage with parameters brick and mortar and linear elements, which were modeled reinforcement of smooth bars or truss type reinforcement.
- Stage III. Displacement of *k* nodes ($x_k^{II}, y_k^{II}, z_k^{II}$) obtained from the solution of models of stage II was loaded the micromodels with overall dimensions 278×310×250(125) mm. Methods of discretization of numerical models in stages II and III are shown in Figure 2.

ISSN: 2454-1907
DOI: 10.5281/zenodo.1412216

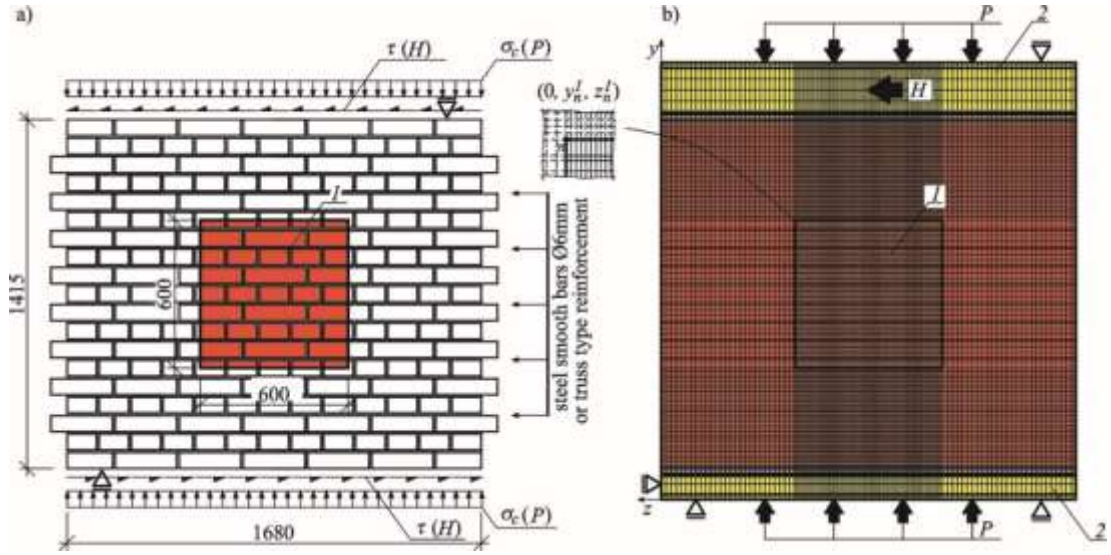

Figure 1: Masonry walls: a) test specimens [22, 23], b) numerical macromodel - stage I, (*1* – wall fragment under analyzed 600×600 mm, *2* – element of the test stand)

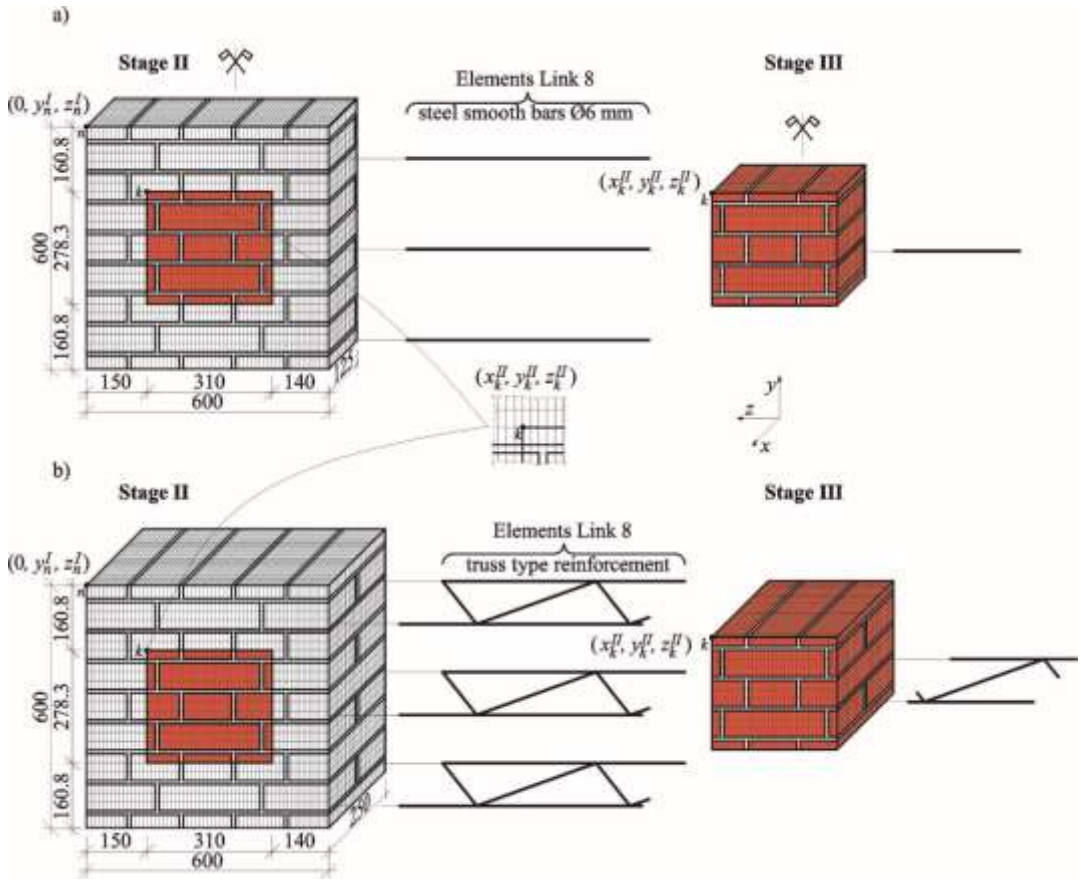

Figure 2: The geometry of the models and mesh of finite elements numerical models used in the calculation (stage II and III): a) elements of reinforced with bars, b) the elements of reinforced with truss type reinforcement

ISSN: 2454-1907
DOI: 10.5281/zenodo.1412216

2.2. Material Models of Mortar and Brick in Stage Iii

Elastic-brittle material model with the failure surface of the Willam-Warnke (WW-5) [24,8,26,25] was used for mortar and bricks, the shape of the octahedral stress [27] shown in Figure 3. Meridians of the five parameters surface cone are parabolic in shape (Fig. 4). In the deviatoric cross-sectional shape of the failure surface WW-5 consists of three mutually tangent to the ellipse described an equilateral Rankine equilateral triangle and inscribed the outer circle Drucker-Prager. Meridian where is located the point corresponding to the compressive strength f_c the uniaxial state of stress is called compression meridian and the meridian which is located the uniaxial tensile strength f_t and biaxial compression f_{cc} called tension meridian. In the deviatoric cross-section shape of the surface is periodic - meridians on the surface are alternately rotated through Lode angle Θ=60°. All meridians intersect the hydrostatic axis at one point which corresponds to the triaxial tensile strength f_{ttt} [110].

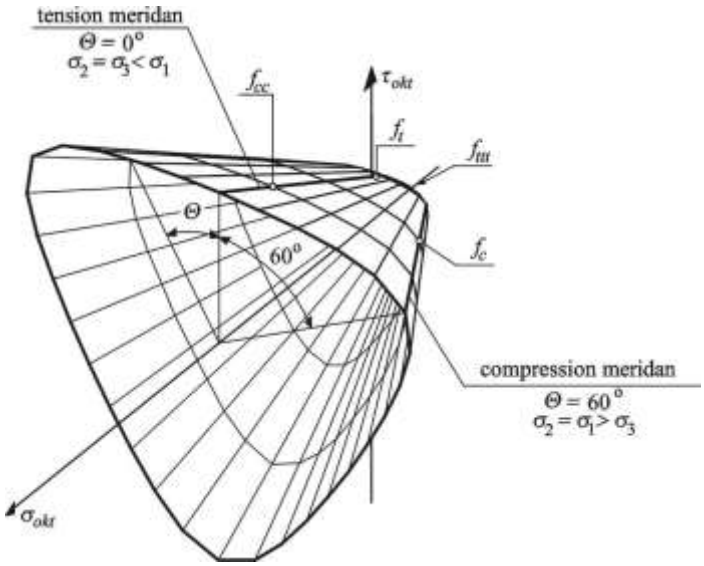

Figure 3: Willam-Warnke (WW-5) failure surface

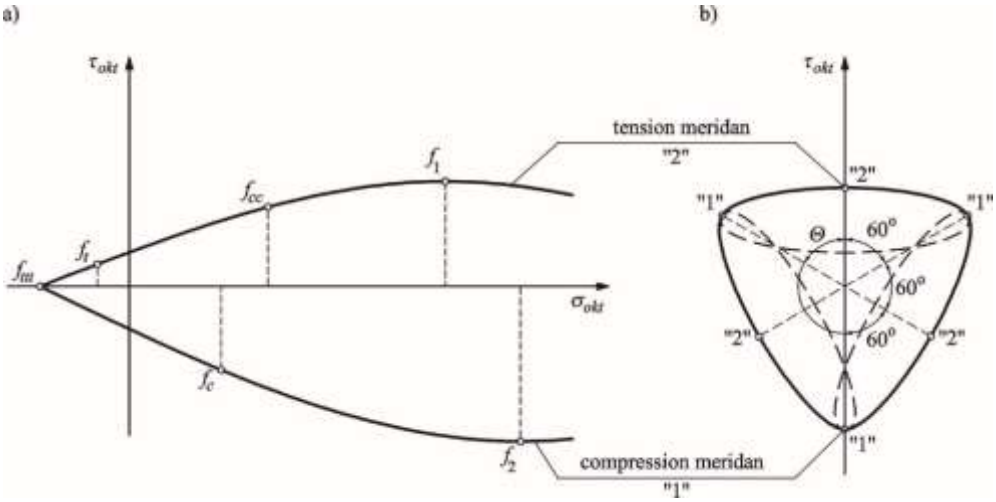

Figure 4: Willam-Warnke (WW-5) failure surface parameters: a) deviatoric cross-section (Θ = 0°), b) hydrostatic cross-section

ISSN: 2454-1907
DOI: 10.5281/zenodo.1412216

Mortar and bricks uniaxial compressive strength and tensile strength f_c, f_t were adopted directly from the research cylinders ϕ 60 × 120 mm. However, biaxial compressive strength was f_{cc} – from the triaxial test, where the samples were destroyed with uniform lateral and vertical compressive stress $\sigma_{ver} = 0$. The results of uniaxial and triaxial tests were plotted on the graph and approximated by polynomials of the second degree least squares method. In addition, the shape of the meridian compression adjustment was made and found a common point of intersection with the tension meridian corresponding to the triaxial tension strength f_{ttt}. The adjusted compression and tensile meridians views WW-5 surface of the mortar and brick is shown in Figure 5 and Figure 6 and summarized in Table 1, where also given modules of elasticity E and Poisson ratios v obtained in the uniaxial study.

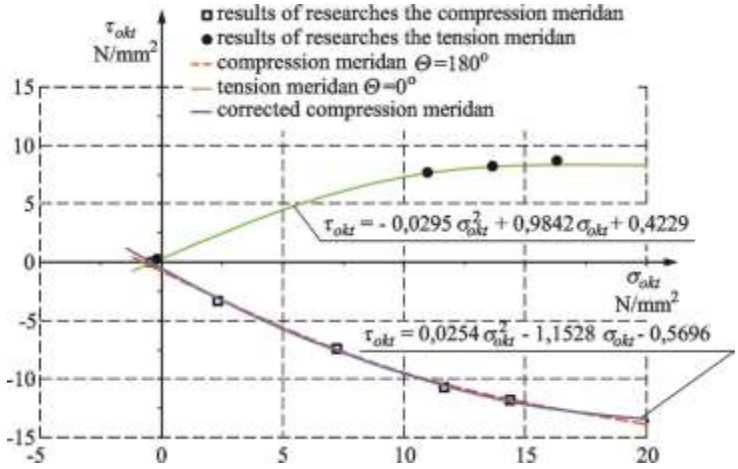

Figure 5: Corrected tensile and compressive meridians of mortar

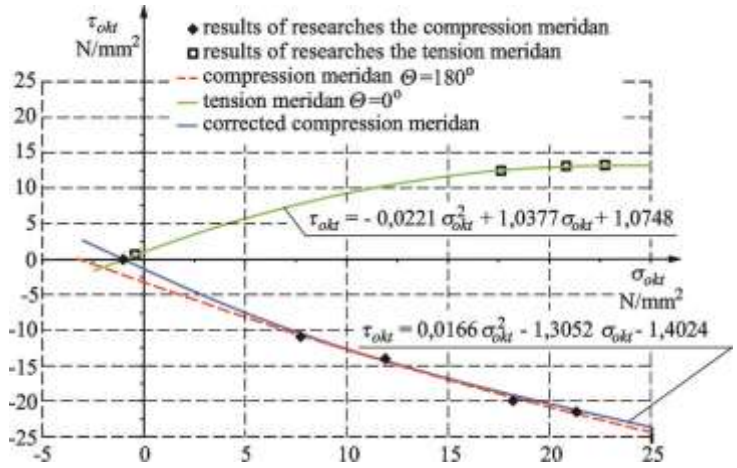

Figure 6: Corrected tensile and compressive meridians of brick

Table 1: The parameters of mortar and bricks taken for numerical computations

Parameter	Mortar	Brick
uniaxial compressive strength f_c, N/mm²	6,77	22,5
uniaxial tensile strength f_t, N/mm²	0,529	1,31
biaxial compressive strength f_{cc}, N/mm²	16,4	26,5
extreme values on the tension meridian f_1, N/mm²	$f_{1,max} = \tau_{okt} = 8,63$	$f_{1,max} = \tau_{okt} = 13,3$
extreme values on the compression meridian f_2,	$f_{2,max} = \tau_{okt} = 13,7$	$f_{2,max} = \tau_{okt} = 27,1$

ISSN: 2454-1907
DOI: 10.5281/zenodo.1412216

N/mm²		
modulus of elasticity *E,* N/mm²	3070	3570
Poisson ratio - ν	0,227	0,131

"Smared band of crack" forming in the direction in accordance with the directions of principal stress was used in the micromodel. After cracking there followed modification of the properties of the finite element. Initially isotropic material (mortar and brick) transformed in orthotropic. One of the axes of the material changed the direction perpendicular to the plane of the crack. In this direction occurred initially material weakness and decreased stress on the tensile strength f_t to the value defined as the ratio of the tensile strength and the coefficient of weakness $T_c = 0.1$.

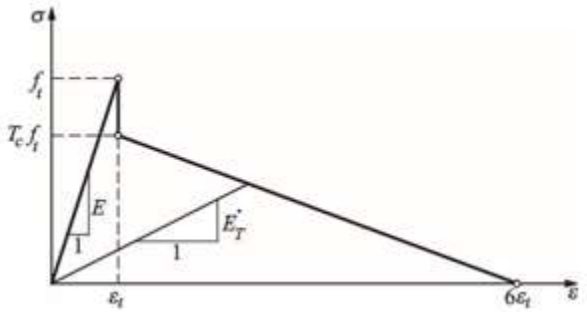

Figure 7: Smeared band of cracks σ – ε relationships

Then the material weakness in the crack described as a function was decreasing linear relationship between tensile strain $\varepsilon_t \div 6\varepsilon_t$. After cracking in subsequent iterations secant modulus E_T was taken. Relationships tensile stress – strain in the plane of crack adopted in the numerical model is presented in Figure 7. In the case of cracks, which occurred in the tensile stress (open crack) with the ability to transfer shear stresses, determined the value of the coefficient β_t (shear transfer coefficient) taking values between 0 to 1. ,,Closed cracks" was similarly given to the properties. Transferring shear coefficient stress ratio defined as a β_c, whose value in the case of open cracks could adopt values between 0 to 1. Both coefficients β_t and β_c assumed equal to 0.6. The cracking due to compression (,,crushing cracks ") were accepted the total degradation of modulus of elasticity of the material, and cracked finite element was losing the ability to transfer any tension.

2.3. Interface Elements

To the reflect the slip occurring at the interface between bricks and mortar observed in the studies [22], it was decided to use the interface elements. Were applied as 10 nodes surface interface elements of Target 174-Contac 170 type available in the ANSYS system - figure 8.

Elements were elastic-plastic (with the weakening) characteristics of the load-displacement - Figure 9 under shear load. Displacements increased proportionally with an increase of load in the elastic range. Weakness - slip represented by the degradation of the static friction coefficient of friction value to the residual friction coefficient of friction occurred after reaching the shear strength. Elements have limitations solely due to tension which meant that when the value of the tensile stresses in the joint exceed the limit was followed separation of connected pre-contact surfaces (mortar - brick) in the case of normal stress.

ISSN: 2454-1907
DOI: 10.5281/zenodo.1412216

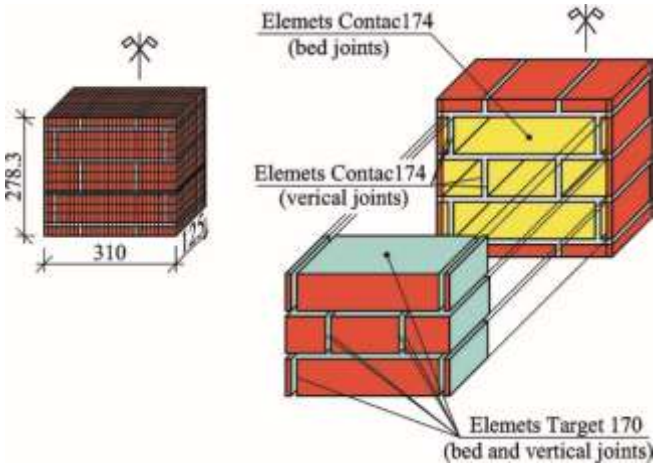

Figure 8: Location interface elements in the micromodel (Stage III)

At the maximum compressive and tensile stress contacting surfaces have remained connected, which means there is an ability to transfer normal and shear stresses. The relationships load (H) - displacement (u) need the following initial value of the shear stiffness K_{s0} in the elastic state.

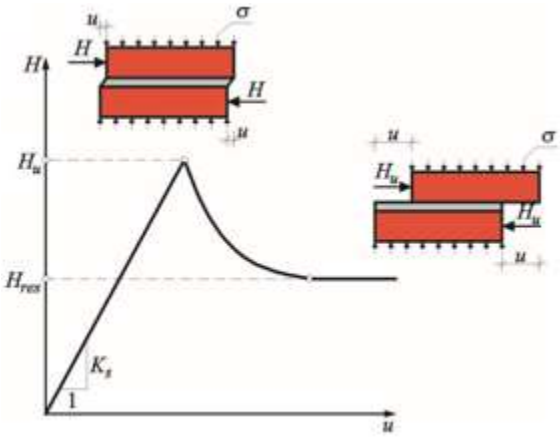

Figure 9: Shear characteristic of interface elements (Stage III*)*

To determine the shear strength (f_v) it was necessary to determine the initial shear strength (f_{vo}) and static coefficient of friction (tgα) in the mortar joints. Coulomb-Mohr (C-M) (1) relationships, as a criterion of shear stress, was used.

$$f_v = f_{vo} + tg\alpha\sigma \tag{1}$$

The shape of the interface elements the shear criteria are shown in Figure 10. Linear relationship (1) was valid in the range of the normal stress σ greater than the tensile strength f_t of the contact to the shear stress not more than $f_{vmax} = 10^{19}$ N/mm^2. Decay coefficient d_c - Figure 10b was used to define after cracking the contact was required. Degradation of the static friction coefficient tgα to the residual coefficient of friction μ_{res} was described in the course of the exponential relationship.

ISSN: 2454-1907
DOI: 10.5281/zenodo.1412216

$$\mu = \mu_{res}\left[1+\left(\frac{tg\alpha}{\mu_{res}}-1\right)e^{-d_c u}\right]. \quad (2)$$

Parameters interface elements necessary to calculate the shear were determined on the basis of the initial shear strength of the wall according to EN-1052-3:2003 *Methods of test for masonry - Part 3: Determination of initial shear strength* code. Interface elements parameters in vertical planes were determined by dividing the value of the parameter (except for the d_c coefficient) and quality factor [28] ("quality factor"), which was adopted equal to 0.5. Parameters of the interface elements shown in Table 2.

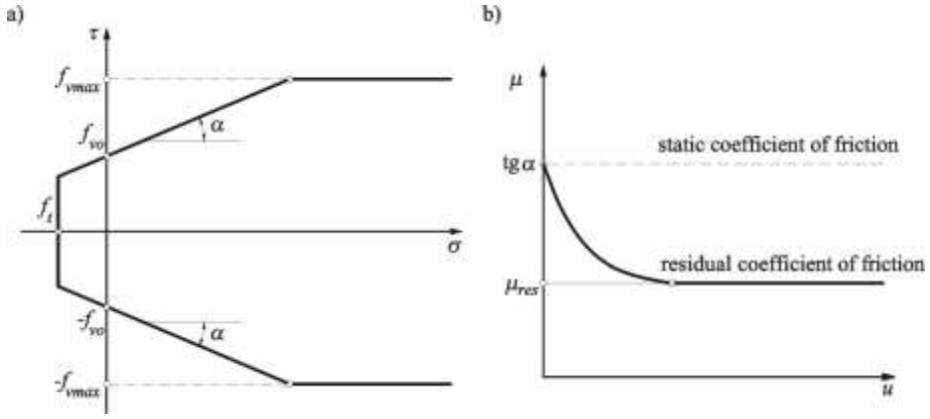

Figure 10: Interface elements failure criteria: a) τ – σ relationships, b) graphic illustration of the decay coefficient of friction d_c

Table 2: Parameters of interface elements

Parameter	**Bed joints**	**Vertical joints**
initial stiffness of shear wall K_s, kN/mm	138	69
initial shear strength (cohesion) f_{vo}, N/mm^2	0,452	0,226
static coefficient of friction $tg\alpha$	1,06	0,503
maximum tensile stress in the contact f_t,N/mm^2	0,011	0,006
residual coefficient of friction μ_{res}	0,845	0,422
decay coefficient d_c	0,030	0,030

2.4. Steel Material Model

Reinforcing bars in the model were modeled using discrete links, with elastic-plastic characteristics. Huber-Mises-Hencky yield surface in the octahedral system coordinate stress is infinitely long cylindrical surface - Figure 11 was applied. Bilinear relationship stress - strain, with associated flow law and the Prandtl-Reuss kinematic strengthening law and was applied. The kinematic strengthen law takes into account the change of the position of the plasticity surface stress in compression due to caused by tension, the so-called Baushinger effect - Table 3.

ISSN: 2454-1907
DOI: 10.5281/zenodo.1412216

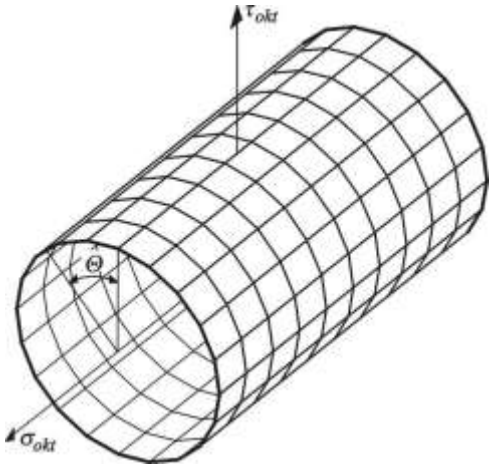

Figure 11: Huber-Mises-Hencky yeld furface ([27])

Table 3: Mechanical properties of reinforcing steel

Reinforcement and diameter mm	**Parameter**			
	E_s **N/mm²**	**Poisson ratio**	$R_{p0,2}$ **N/mm²**	E_T **N/mm²**
smooth bars ϕ 6	170000	0.3	592	1590
strip of truss ϕ 5	183000		701	1090
bracking of truss ϕ 3,75	176000		625	742

E_s - modulus of elasticity, $R_{p0,2}$ - yield stress, E_T, - secant modulus.

3. The Results and Analysis of the Researches and Numerical Calculations

Mean values of cracking $H_{cr,mv}$ and ultimate forces $H_{u,mv}$ obtained on all series specimens (described in detail in the work [22]) are shown in Table 4. The results of the numerical calculations as a cracking $H_{cr,cal}$ and ultimate $H_{u,cal}$ forces numerical models used in stage III are shown as well. Numerical shell models in stage I loaded with the forces of the average values specified at the time of the destruction of the research elements $H_{u,mv}$ - Table 4.

The result of model calculations carried out in the first stage was to determine the components of the displacements of all the nodes on the edge of area of 600×600 mm, which linearly elastic mikromodel charged in stage II, these displacements has been loaded with linearly elastic micromodel in stage II. Displacements of nodes in stage II model obtained along the edge of the model (278×310×250 (125) mm) in stage III was used. Comparison of shear load *H* non-dialatational strain angle Θ tests specimens, at the σ_c = 1.5 N/mm^2 initially compressions and numerical micromodels used in the phase III are shown in Figure 12.

Strains angle research elements grew in almost direct proportion to the shear loads to load values of 80% $H_{cr,mv}$. The highest stiffness characterized by elements reinforced with truss type reinforcement and the lowest stiffness was unreinforced specimens. With the increase of shear load *H* disproportionate increase angle displacements were visible, especially important after cracking. The reinforced numerical models characterized by greater stiffness than the unreinforced walls.

ISSN: 2454-1907
DOI: 10.5281/zenodo.1412216

Table 4: Mean values of cracking and ultimate forces

Series	**reinforcement ratio ρ_h %**	**σ_c N/mm^2**	**Researches [22]**		**FEM model**		$\frac{H_{cr,mv}}{H_{cr,cal}}$	$\frac{H_{u,mv}}{H_{u,cal}}$	$\frac{H_{cr,mv}}{H_{u,cal}}$
			Cracking forces	**Ultimate forces**	**Cracking forces**	**Ultimate forces**			
			$H_{cr,mv}$ kN	**$H_{u,mv}$ kN**	**$H_{cr,cal}$ kN**	**$H_{u,cal}$ kN**			
Unreinforced specimens	0	0*	144	163	144	191	1,00	0,85	0,75
		0,5	287	341	--	--	--	--	--
		1,0	375	445	--	--	--	--	--
		1,5*	424	567	181	416	2,34	1,36	1,02
Reinforced with steel smooth bars	0,05	0	186	237	--	--	--	--	--
		0,5	326	448	--	--	--	--	--
		1,0	396	542	--	--	--	--	--
		1,5	407	584	--	--	--	--	--
	0,1	0*	201	234	167	282	1,20	0,83	0,71
		0,5	335	475	--	--	--	--	--
		1,0	415	585	--	--	--	--	--
		1,5*	441	668	200	585	2,21	1,14	0,75
Reinforced with with truss type reinforcement	0,05	0	310	333	--	--	--	--	--
		0,5	391	462	--	--	--	--	--
		1,0	512	668	--	--	--	--	--
		1,5	580	739	--	--	--	--	--
	0,1	0*	321	348	193	415	1,66	0,84	0,77
		0,5	462	542	--	--	--	--	--
		1,0	538	685	--	--	--	--	--
		1,5*	609	743	225	576	2,71	1,29	1,06

* - models analyzed in numerical calculations

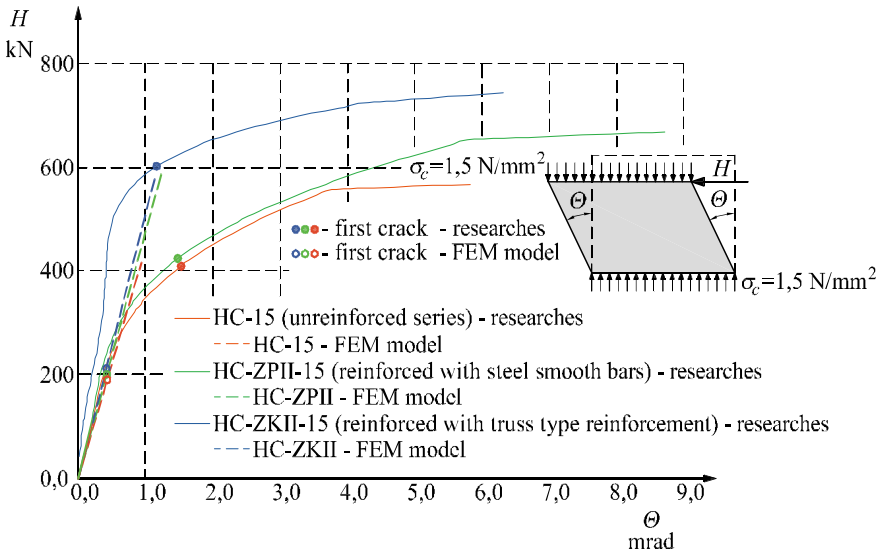

Figure 12: Comparisons of shear load – non-dilatational strain angle (H-Θ) research series elements and numerical models

ISSN: 2454-1907
DOI: 10.5281/zenodo.1412216

Due to the modeling strategy in stage III used loaded displacements of nodes obtained from the models in stage I and stage II did not occur proportional increase of walls angle deformation after crcking, and the difference of destructive forces $H_{u,cal}$ and given in the researches $H_{u,mv}$ was $H_{u,cal}$ / $H_{u,mv}$. However, size of the numerical micromodel (stage III) model, allows for comparison of the cracking forces specimen's models $H_{cr,mv}$ to the ultimate forces of numerical models $H_{u,cal}$ ($H_{u,cal}$ / $H_{cr,mv}$ = 0,77 – 1,06). Selected results of numerical models sheared horizontally and compressed vertically at σ_c = 1,5 N/ mm^2 reinforced with steel smooth bars and truss type reinforcement are presented later in this chapter.

3.1. Cracking and Destruction

In the model reinforced with bars, cracks were first observed at a force of $H_{cr,cal}$ = 200 kN N/mm^2, which is considerably less by about 120% compared to the average force $H_{cr,mv}$ = 441 kN strength obtained in research. The first cracks – fig. 13a,b formed in the bed joint above of corner the bricks placed in head layers. Where there was the reinforced bar present cracking intensity was significantly lower than in areas without reinforcement mortar.

Destruction of the model was observed at a force of $H_{u,cal}$ = 585 kN of 14% less than the obtained in experimental studies $H_{u,mv}$ = 668 kN. The increase in load resulted in the progressive development of the cracking areas (fig. 13c,d) including internal joint and bricks. At the time of the near destruction of large cracking covered almost all the internal joint head, the supporting brick and joint. In the areas where reinforcement is used, the intensity at the time of destruction of cracking was slightly smaller. However, near to the face of the wall there have more damage and secondary cracks (blue and green in the present step load) providing a clear overload these areas.

Reinforcement strains were also analyzed in the following phases of the load (Figure 14).

After an initial compression to the, the σ_c = 1,5 N/mm^2 the deformation of the reinforced bar located in the bed joint formed to the uniform tension. With the increase of the horizontal load, the deformations of reinforcement were reduced and their distribution on the length of the bar becomes distorted. After cracking, as the rise of the horizontal load on part of the bar situated at the location cracked bed joint tensile deformation occurred the rest of the bar located in the non-cracked bed joint compressive deformation occurred.

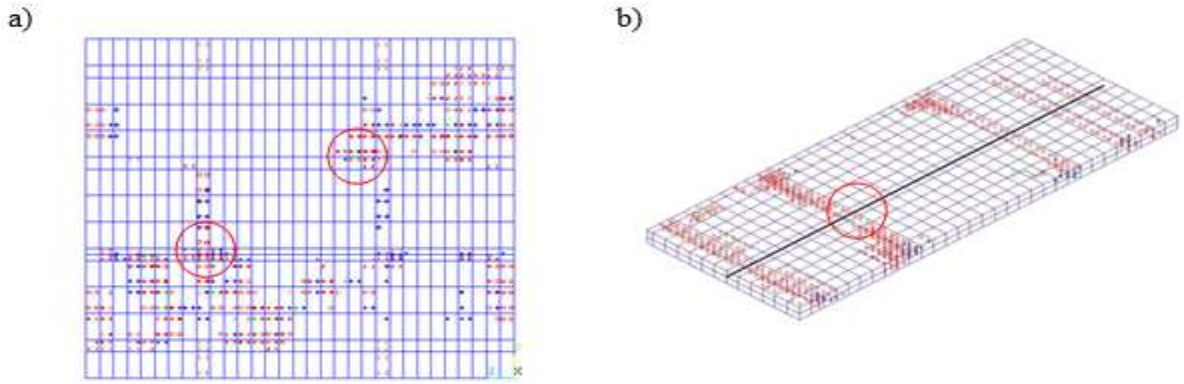

ISSN: 2454-1907
DOI: 10.5281/zenodo.1412216

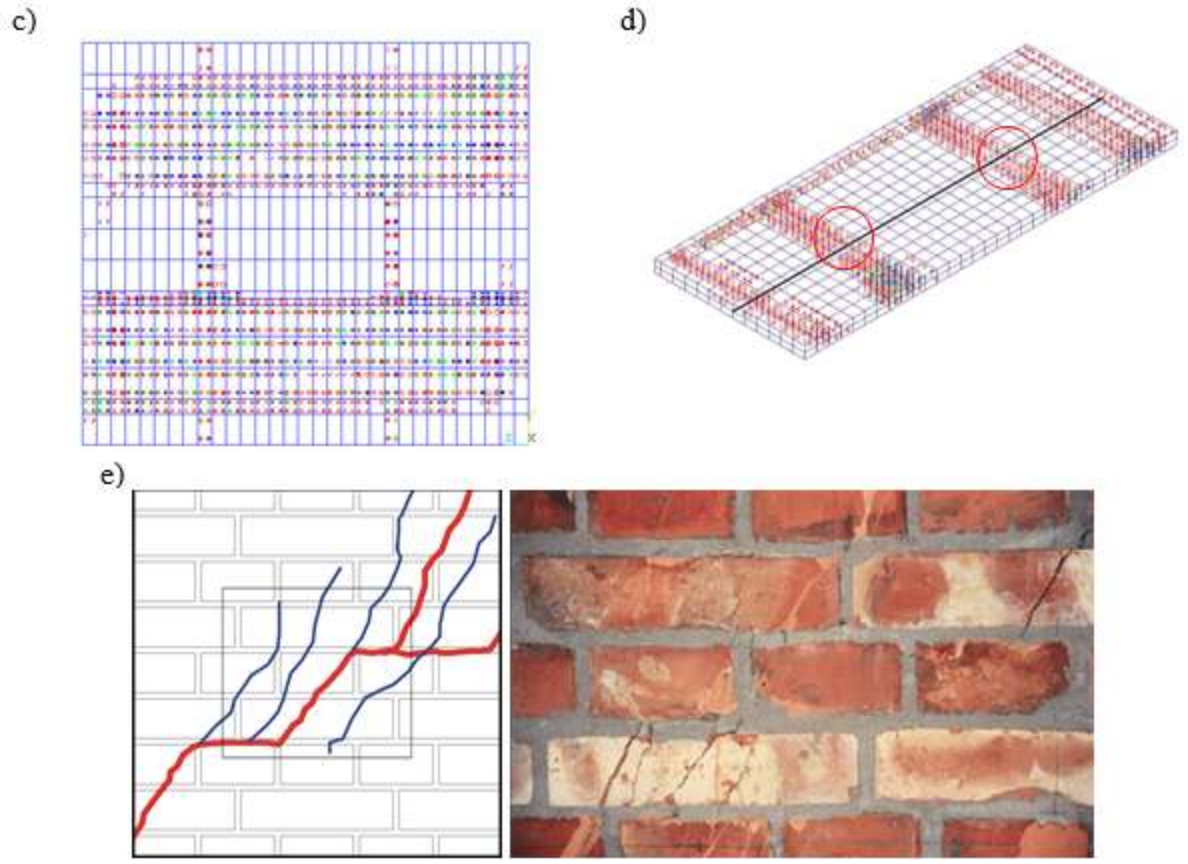

Figure 13: Cracking patterns of reinforced with smooth bars model HC-ZPII-15 series a) numerical model - view from the face of the wall ($H_{cr,cal}$), b) numerical model - view of the bed joint with the steel bar ($H_{cr,cal}$), c) numerical model - view from the face of the wall ($H_{u,cal}$), d) numerical model - view of the bed joint with the steel bar ($H_{u,cal}$), e) cracking of lab element

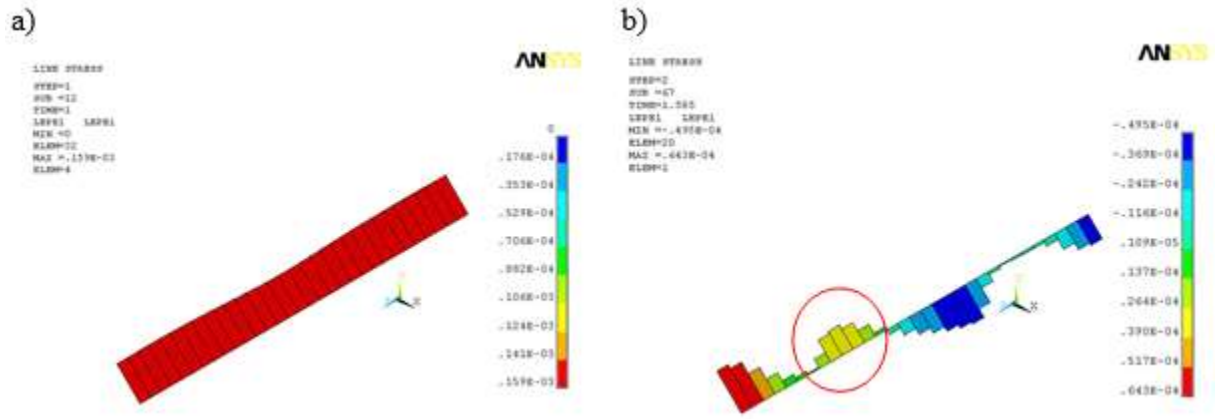

Figure 14: Strains of the steel smooth bar □6 mm in successive phases of the load HC-ZPII-15 series: a) initial compression H = 0 kN, b) the destruction of model $H_{u,cal}$ = 585 kN

In the numerical model reinforced with truss type reinforcement cracks were first observed at a load of $H_{cr,cal}$ = 225 kN, or approximately 171% less than that obtained in the research. The first

ISSN: 2454-1907
DOI: 10.5281/zenodo.1412216

visible cracks (Figure 15a, b) of the wall reinforced with steel truss type reinforcement was also observed in the area underlying the bed joint corner of brick, and in places a connected bracking and strip of truss. The destruction occurred at the load and $H_{u,cal}$ = 576 kN and was 29% lower than obtained in the lab model $H_{cr,mv}$ = 609 kN. In addition, the cracks were visible in bed and vertical joint (figure 15c, d). With the increase of horizontal load to a growing area of cracking, bed joints and cracks also appear in the bricks. At the time of the destruction cracking covered almost all the head joint. As in the case of walls with steel bars, in places where the truss type reinforcement was located cracking intensity was less than the near the face of wall. Initial deformation of the truss bars, like the smooth bars were tensile and uniform– figure 16a.

With increasing horizontal load there was seen a gradual reduction in strain in bars and change the distribution of the length. On the sections and diagonal bracking and belts lying cracked areas in the bed joints increased tensile strain – fig. 16b after the cracking. At the time of the destruction, strains were significantly changed in relation to the intermediate states. In the place the mortar cracking dominated tensile strains belts and diagonal bracking, while in places where the mortar remains non-cracked compressive strains occurred. Due to the free of the wall deformation in the thickness direction (along the x axis) the greatest strains diagonal bracking was observed.

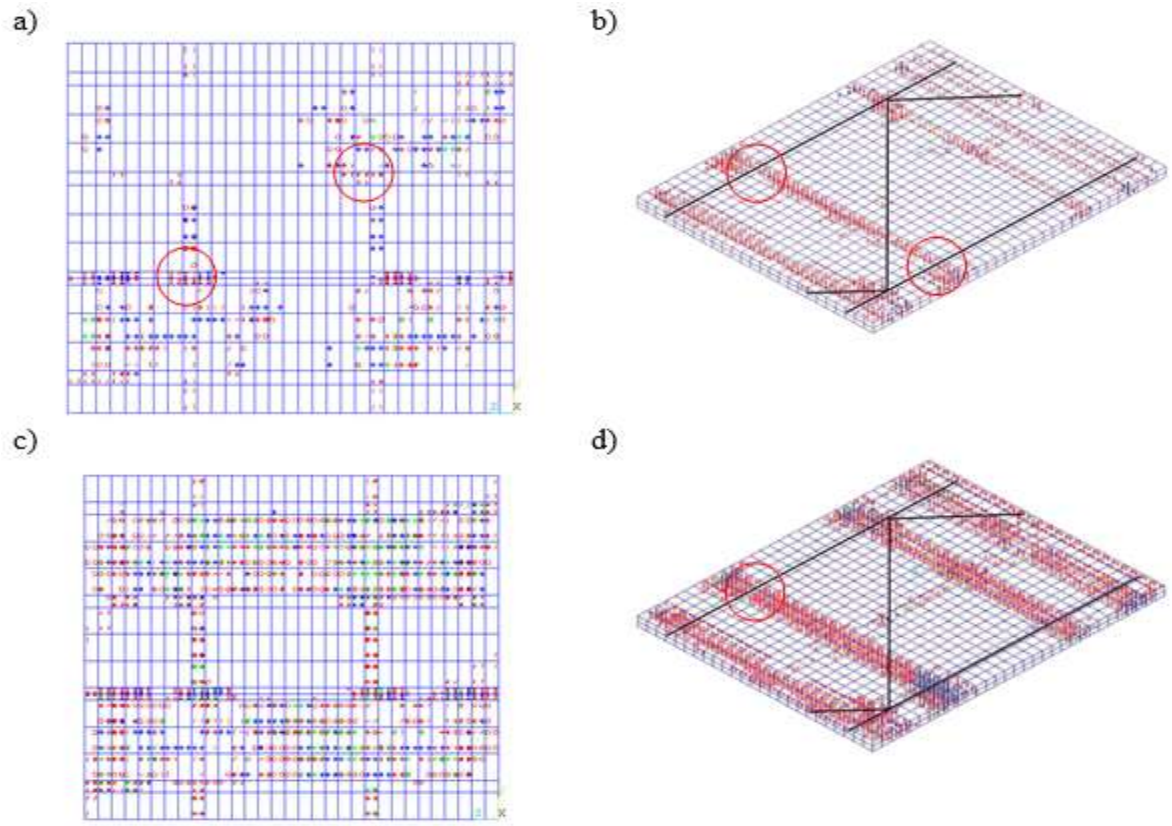

Figure 15: Cracking patterns of reinforced with smooth bars model HC-ZKII-15 series
a) numerical model - view from the face of the wall ($H_{cr,cal}$), b) numerical model - view of the bed joint with the truss type reinforcement ($H_{cr,cal}$), c) numerical model - view from the face of the wall ($H_{u,cal}$), d) numerical model - view of the bed joint with truss type reinforcement ($H_{u,cal}$), e) cracking of lab element

ISSN: 2454-1907
DOI: 10.5281/zenodo.1412216

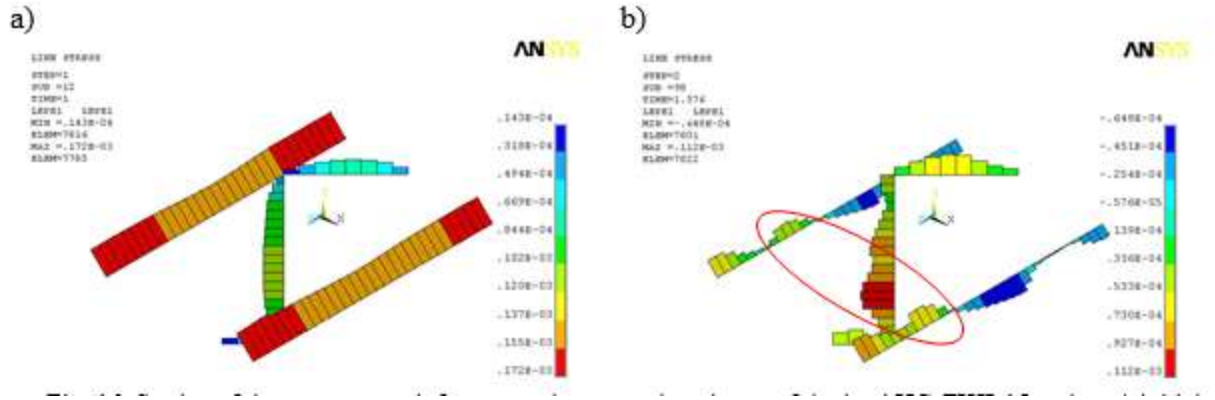

Figure 16: Strains of the truss type reinforcement in successive phases of the load HC-ZKII-15 series: a) initial compression H = 0 kN, b) the destruction of model $H_{u,cal}$ = 576 kN

3.2. Bed Joints Deformation

A comparison of longitudinal joint strains was also carried out where reinforcement was introduced and compared with models unreinforced. Figures - fig 17a, 18a and 19a show a map of the longitudinal strains of the bed joint at cracking and in Figures 17b, 18b and 19b show the longitudinal strains visible form the face of the model.

The bed joint areas, which were observed first cracks (masonry unit corners) in the joint without reinforcement can be seen the concentration of strain. However, in the joints, in which the reinforcement introduced strain distribution in these areas was different in terms of distribution and deformation values. Significant changes have occurred in places where the bars crossed an area of concentration, the strain decreased of 20% to 50%. In this case the separation of the mortar from bricks was visible only on the head surfaces. The visible reduction of mortar strains in the bed joints was the reason for reduced damages around bars and increase of cracking load and stiffness with respect to unreinforced masonry.

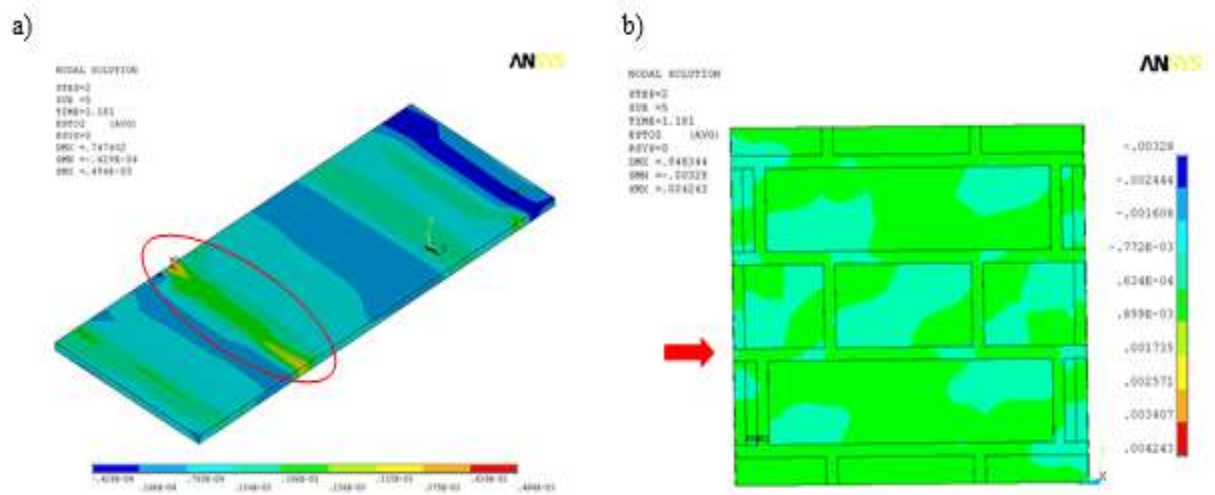

Figure 17: Longitudinal strain ε_z of unreinforced masonry $H_{cr,cal}$ = 181 kN HC-15 series: a) bed joint, b) face of model

ISSN: 2454-1907
DOI: 10.5281/zenodo.1412216

3.3. Principal Stress in the Brick

According to the well-known Mann-Muller model [28, 29] for shear and compression masonry units can be cracked if the principal stress exceeds the tensile strength. The following figures (fig. 20, 21, 22) presented maps of principal stresses σ_1 ($\sigma_1 > \sigma_2 > \sigma_3$) visible on the surfaces of the bricks located above and below the reinforced bed joint. Comparisons were made at a force equivalent to a cracking of unreinforced model HC-15 series ($H_{cr,cal}$ = 181 kN). The most significant changes occurred in the state of stress bricks placed longitudinally in the wall. When applied reinforcement was visible, a shift (and increase in value) of extreme stress in the direction of the face of the wall surface in relation to the bricks placed in the model without reinforcement, where the extreme values were almost the entire width of the bricks. This phenomenon substantially reduced the loads of bricks cracking inside the wall, but in turn, caused the cracks near the face surface of the wall. The bricks placed transversely reinforcement effect was much less noticeable.

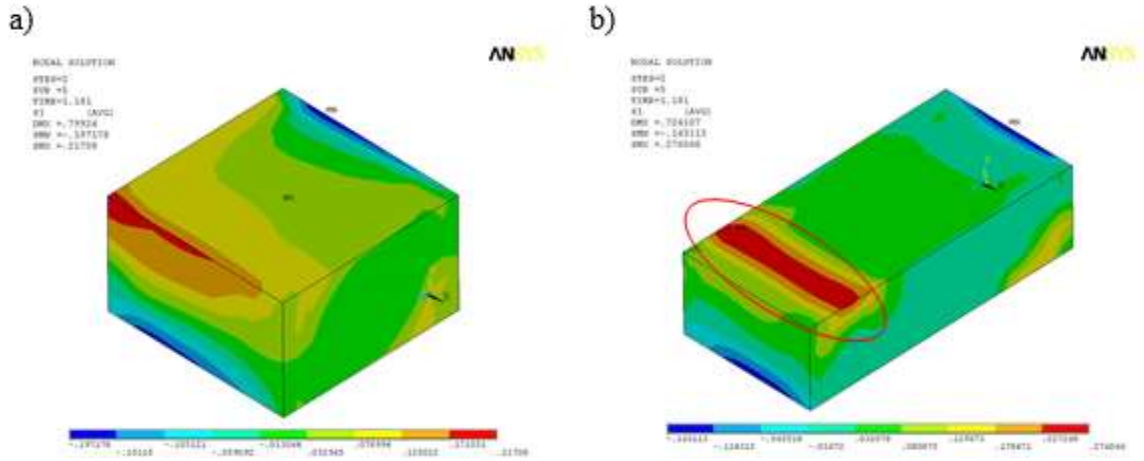

Figure 20: Principal stress σ_1 in brick of unreinforced wall (HC-15) $H_{cr,cal}$ = 181 kN: a) brick over reinforced bed joint, b) brick below reinforced bed joint

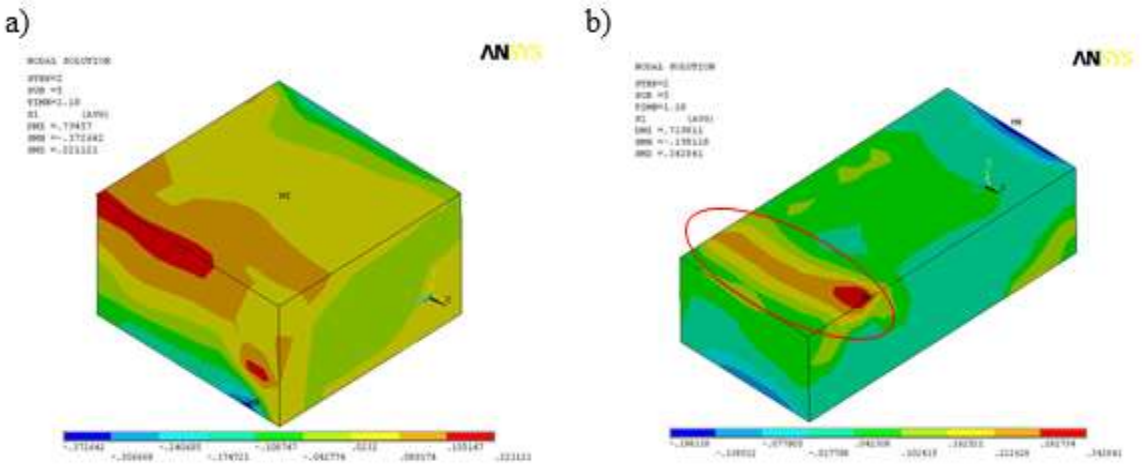

Figure 21: Principal stress σ_1 in brick of wall reinforced with smooth bars (HC-ZPII-15) $H_{cr,cal}$ = 180 kN: a) brick over reinforced bed joint, b) brick below reinforced bed joint

ISSN: 2454-1907
DOI: 10.5281/zenodo.1412216

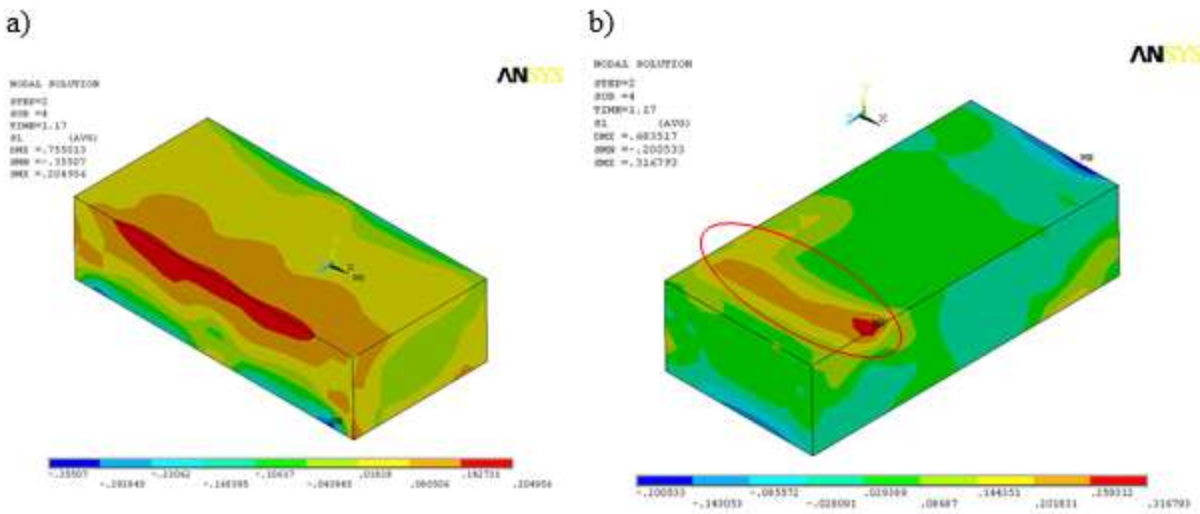

Figure 22: Principal stress σ_1 in brick of wall reinforced with truss type reinforcement (HC-ZKII-15) $H_{cr,cal}$ = 170 kN: a) brick over reinforced bed joint, b) brick over reinforced bed joint

4. Summary and Conclusions

FEM calculations were performed to formulate the following conclusions:

1) In the analysis of large masonry structures is possible use the masonry micromodel part of the wall and loading external supports deformities (obtained from FEM calculations macro model of the wall) on condition:

- the proper determination of mechanical parameters of wall macro model,
- application of failure and plasticity surface and interface finite elements on surface contact the masonry units and mortar.

2) The method of structural analysis consisting of separating of the wall area and calculating it as a discrete micro model can describe the work of the wall until cracking the real wall. This method of modeling were obtained:

- destructive forces of $H_{u,cal}$ of micro models, determining with reasonable accuracy cracking the real only sheared walls (σ_c =0 N/mm^2) $H_{cr,mv}/H_{u,cal}$ = 0,71÷0,77 and the sheared and maximum compressed (σ_c = 1,5 N/mm^2) $H_{cr,mv}$ / $H_{u,cal}$ = 0,75÷1,02,
- the cracking forces of $H_{cr,cal}$ considerably smaller than the value obtained in the researches $H_{cr,mv}$ the only sheared elements (σ_c = 0 N/mm^2) $H_{cr,mv}$ / $H_{u,cal}$ = 1,0÷1,66, and the shear and maximum compressed (σ_c = 1,5 N/mm^2) $H_{cr,mv}$ / $H_{u,cal}$ = 2,21÷2,71,
- relationship load (H) – non-dilatational strain angle (Θ) was similar to the results of research only the cracking.

3) A numerical micro model of masonry confirmed the influence (qualitatively) of the applied reinforcement on the mechanism of cracking formation;

- cracking each time were created in the same areas of mortar - in the bed joint located at the corners of brick
- confirmed the overall variability of the observed deformation of the reinforcement obtained in the researches. However, due to limitation of displacements of external supports of the model was not observed creation the tensile reinforcement strains observed in studies the real wall,

ISSN: 2454-1907
DOI: 10.5281/zenodo.1412216

- longitudinal strains the bed joint mortar were significantly reduced in places where it was placed reinforcement,
- significant reductions in the lateral deformation of mortar in the bed joint observed in the case of truss type reinforcement,
- applied reinforcement changed the value of the largest principal stress on the visible surfaces of bricks placed longitudinally in the wall,
- load value at which cracking was observed of the numerical models was significantly lower than that observed in studies,
- value of the failure load of the horizontal walls of the numerical models was similar to the value of cracking loads obtained in experimental studies.

References

[1] Lourenço P.B., Rots J.G., Blaauwendraad J.: Two Approaches for the Analysis of Masonry Structures: Micro and Macro-Modeling. Heron. Vol. 40, No. 4, 1995, pp. 313 ÷ 340.
[2] Lourenço P.B.: Two Aspect Related to the Analysis of Masonry Structures: Size Effect and Parameter Sensibility. TNO. Building and Construction Research 1997.
[3] Lourenço P.J.B.B.: Computational Strategies for Masonry Structures. PhD Thesis. Delf University Press. 1996.
[4] Shing P.B., Cao L.: Analysis of Partially Grouted Masonry Shear Walls. U.S. Department of Commerce National Institute of Standard and Technology Building and Fire Research Laboratory. Gaithersburg, MD 20899. Report NIST GCR 97-710, 1997.
[5] Sieczkowski J., Szołomicki J.: Metody komputerowej analizy konstrukcji murowych. Inżynieria I Budownictwo Nr 7 / 1998, pp. 376 ÷ 379.
[6] Sieczkowski J., Szołomicki J.: Metody obliczeń statyczno-wytrzymałościowych sklepień w budynkach gotyckich. Oficyna Wydawnicza Politechniki Wrocławskiej. Wrocław 1999.
[7] Szojda L.: Analiza numeryczna współdziałania murowanych budynków ścianowych z deformującym się podłożem. Praca Doktorska. Gliwice 2001.
[8] Drobiec Ł.: Analiza murów z cegły pełnej ze zbrojeniem w spoinach wspornych poddanych obciążeniom pionowym. PhD Thesis. Gliwice 2004.
[9] Lourenço P.B., Rots J.G.: An Anisotropic Failure Criterion Suitable for Numerical Implementation. Proceedings of 7th North American Masonry Conference, 2 ÷ 5 June 1996, University of Notre Dame, South Bend, Indiana, pp. 282 ÷ 293.
[10] Lourenço P.B.: Anisotropic Softening Model for Masonry Plates and Shells. Journal of Structural Engineering. Vol. 126, No. 9, September 2000, pp. 1008 ÷ 1016.
[11] Szojda L.: Możliwości analizy numerycznej konstrukcji murowej. XLVII Konferencja Naukowa Komitetu Inżynierii Lądowej i Wodnej PAN i Komitetu Nauki PZITB. Opole-Krynica 2001. Tom 3, pp. 385 ÷ 392.
[12] Szojda L., Majewki S.: Analiza numeryczna sił wewnętrznych w budynku murowanym pod wpływem deformacji terenu. XLIX Konferencja Naukowa Komitetu Inżynierii Lądowej i Wodnej PAN i Komitetu Nauki PZITB. Warszawa-Krynica 2003. Tom 4, pp. 163 ÷ 170.
[13] Kubica J. Ściany z cegły w złożonym stanie naprężenia. PhD Thesis. Gliwice, 1995.
[14] Kubica J.: Numerical Modelling of the Vertical Shearing Masonry Walls. Proceedings of 11th International Brick / Block Masonry Conference, 1997 14 ÷ 16 October, Shanghai, pp. 1229 ÷ 1238.
[15] Ciesielski R.: Wykorzystanie teorii konstrukcji inżynierskich w analizie historycznych budowli zabytkowych. IV Konferencja Naukowo-Techniczna. Inżynierskie Problemy Odnowy Staromiejskich Zespołów Zabytkowych. Kraków 21 ÷ 23 Maja 1998r. Tom III, pp. 57 ÷ 74.

ISSN: 2454-1907
DOI: 10.5281/zenodo.1412216

[16] Wrana B.: Metody Numeryczne w analizie konstrukcji budowli zabytkowych. IV Konferencja Naukowo-Techniczna. Inżynierskie Problemy Odnowy Staromiejskich Zespołów Zabytkowych. Kraków 21 ÷ 23 maja 1998, Tom III, pp. 41 ÷ 48.
[17] Wrana B.: Problemy Modelowania i Analizy Numerycznej Murów. V Konferencja Naukowo-Techniczna. Inżynierskie Problemy Odnowy Staromiejskich Zespołów Zabytkowych. Kraków 17 ÷ 19 maja 2000, Tom I, pp. 245 ÷ 258.
[18] Lopez J., Oller S., Onnte E., Lubliner J.: A Homogeneous Constitutive Model for Masonry. International Journal for Numerical Methods in Engineering. Vol. 46, 1999, pp. 149 ÷ 156.
[19] Majewski S., Wandzik G., Klemczak B., Szojda L.: Numerical Analysis of Reinforced Masonry Walls Subjected to the Influence of Mining Ground Subsidence. Proceedings of 7th North American Masonry Conference. June 2 ÷ 5, 1996. University of Notre Dame-South Bend, Indiana, USA. Vol. I, pp. 559 ÷ 570.
[20] Merlet J.D.: Reinforced Masonry Made of Hollow Units: Finite Element Modelling, Development and Validation. Wall Structures. 29th Meeting, W23 CIB. Padua, October 1992, pp. 67 ÷ 88.
[21] Cerioni R., Donida G.: A Finite Element Model for the Nonlinear Analysis of Reinforced and Prestressed Masonry Walls. Computers and Structures. Vol. 53, No. 6, pp. 1291 ÷ 1306.
[22] Jasiński R.:,, Study of reinforced clay brick masonry walls horizontally sheared" 8th International Masonry Conference, Dresden 2010, pp. 1231 ÷ 1242.
[23] Jasiński R.: Nośność i odkształcalność zbrojonych ścian murowych ścinanych poziomo. PhD Thesis. Gliwice 2005.
[24] Brencich A., Corradi C., Gambrotta L., Mantegazza G., Sterpi E.: Compressive Strength of Solid Clay Brick Masonry under Eccentric Loading. Proceedings of 6th International Masonry Conference. Proceedings No. 9, London 2002, pp. 37 ÷ 46.
[25] Jäger W., Schöps P.: Numerical Modeling of Masonry Under Shear Loading. Proceedings of 13th International Brick / Block Masonry Conference, 2004 4 ÷ 7 July, Amsterdam.
[26] Drobiec Ł.: FEM micro model of Masonry. 5th International Conference AMCM 2005, Gliwice-Ustroń, Poland, 2005.
[27] Majewski S.: Mechanika betonu konstrukcyjnego w ujęciu sprężysto-plastycznym. Monografia. Wydawnictwo Politechniki Śląskiej. Gliwice 2003 r.
[28] Dialer Ch.: Some Remarks on The Strength and Deformation Behavior of Shear Stressed Masonry Panels Under Static Monotonic Loading. Proceedings of 9th International Brick / Block Masonry Conference, October 1991, Berlin, pp. 276 ÷ 282.
[29] Müller H.: Untersuchungen zum Tragverhalten von Qerkraftbeanspruchtem Mauerwerk. Bruchverhalten und Bruchtheorie, Auswertung bekannter Sherversuche, Zsätzliche Einflüsse bei Windscheiben. Dissertation, Technischen Hochschule Darmstadt, D17, Darmstadt, 1974.

*Corresponding author.
E-mail address: radoslaw.jasinski@ polsl.pl